Experimental Mechanics (2018) 58:537–547
https://doi.org/10.1007/s11340-017-0371-2

Real-Time Stress Measurement in SiO_2 Thin Films during Electrochemical Lithiation/Delithiation Cycling

S. Rakshit · R. Tripuraneni · S.P.V. Nadimpalli[1]

Received: 18 August 2017 / Accepted: 7 December 2017 / Published online: 10 January 2018

Abstract

Oxide coatings have been shown to improve the cyclic performance of high-energy density electrode materials such as Si. However, no study exists on the mechanical characterization of these oxide coatings. Here, thin film SiO_2 electrodes are cycled under galvanostatic conditions (at C/9 rate) in a half-cell configuration with lithium metal foil as counter/reference electrode, with 1 M $LiPF_6$ in ethylene carbonate, diethyl carbonate, dimethyl carbonate solution (1:1:1, wt%) as electrolyte. Stress evolution in the SiO_2 thin film electrodes during electrochemical lithiation/delithiation is measured *in situ* by monitoring the substrate curvature using a multi-beam optical sensing method. Upon lithiation SiO_2 undergoes extensive inelastic deformation, with a peak compressive stress of 3.1 GPa, and upon delithiation the stress became tensile with a peak stress of 0.7 GPa. A simple plane strain finite element model of Si nanotube coated with SiO_2 shell was developed to understand the mechanical response of the core-shell type microstructures under electrochemical cycling; measured stress response was used in the model to represent SiO_2 constitutive behavior while Si was treated as an elastic-plastic material with concentration dependent mechanical properties obtained from the literature. The results reported here provide insights and quantitative understanding as to why the highly brittle SiO_2 coatings are able to sustain significant volume expansion (300%) of Si core without fracture and enhance cyclic performance of Si reported in the literature. Also, the basic mechanical properties presented here are necessary first step for future design and development of durable Si/SiO_2 core shell structures or SiO_2-based electrodes.

Keywords Silicon dioxide · Lithium-ion battery · In situ stress · Core-shell nanotube · High energy density · Cyclic performance

Introduction

Lithium-ion batteries played a key role in the success of portable electronics. Requirements for clean energy production and low carbon emissions from environmental concerns are driving the advancement of electric vehicle and non-conventional energy production technologies, and lithium-ion batteries are going to play a crucial role in the success of these technologies as well. However, the energy density and capacity of current lithium-ion batteries, which is limited by their electrode materials, are not adequate to meet the future energy demands. Higher capacities can be achieved by replacing the existing electrode materials with high energy density materials. For example, by replacing graphite (anode in the current lithium-ion batteries) with Si, an immediate improvement of 30% on the overall battery capacity can be achieved [1] which is a significant improvement. However, Si and other high energy density anode materials such as Sn and Al suffer from poor cyclic performance due to volume expansion-induced stresses and associated electrode fracture [2–4]. Fracture of electrode particles not only leads to mechanical degradation but also contributes to chemical degradation, because of the formation of solid electrolyte interphase (SEI) layer on fresh fracture surfaces, causing additional capacity loss [5–8].

The SEI layer or passivation layer forms on anode surfaces during charging and discharging cycles due to the decomposition of electrolyte [5, 7]. While this layer imparts kinetic stability to the electrolyte against further reaction in subsequent cycles, it leads to an irreversible loss of Li and battery capacity [9–11]. Most of the capacity loss observed in the first lithiation/delithiation cycle of secondary lithium-ion batteries is due to this SEI layer formation. In general, the SEI layer formation is a self-limiting reaction, i.e., the reaction (or SEI formation) rate decreases significantly after the SEI layer reaches a critical thickness. However, the large volume

✉ S. P. V. Nadimpalli
siva.p.nadimpalli@njit.edu

[1] Department of Mechanical Engineering, New Jersey Institute of Technology, Newark, NJ 07102, USA

changes of Si (or other active) particles during lithiation/delithiation cycles deform or stretch the SEI layer to a critical level and cause the layer to fail. The continuous failure and reformation of the SEI layer during lithiation/delithiation cycles not only causes capacity loss but also leads to an increase in the resistance to Li-ion diffusion (i.e., internal impedance of a battery) [12]. Hence, a chemically and mechanically stable SEI layer is another key factor for improving the cyclic performance of high energy density batteries [5, 7].

Recent studies [13–16] have shown that surface coatings such as SiO_2 on nanoparticles and nanotubes can improve the cyclic performance of high energy density electrode materials by minimizing the mechanical degradation and also stabilizing the SEI layers. It has been hypothesized that the coatings impart chemical stability by isolating the active surfaces from the electrolyte and mechanical stability by preventing volume expansion of the active particle beyond a critical level by constraining or clamping it [13]. It has been argued that the clamping action of SiO_2 potentially minimizes the expansion of Si particles, which reduces the deformation and stress levels in SEI and provides mechanical stability to the SEI layer.

Consequently, SiO_2 coatings on Si with different electrode configurations i.e., core-shell type nanoparticles and nanotubes with solid and hollow core (e.g., see Fig. 1), have been investigated as potential electrode microstructures; SiO_2 coatings on Si [13, 14, 17] and a SiOC coating on Si [18] are some examples. Although SiO_2 was assumed to be inert to lithium, Sun et al. [19] showed that it reacted with Li reversibly resulting in stable capacities of 500 mAh/g for hundreds of cycles. XRD measurements by Chang et al. [20] showed that crystalline SiO_2 is indeed inert and does not react with Li, but amorphous SiO_2 reacts with it due to the valance charge differences in crystalline and amorphous configurations. As a result, in addition to use as a coating material, SiO_2 is also being considered as a potential anode material due to its higher theoretical capacity compared to conventional carbon-based anode materials [19–24].

The capacity of SiO_2 depends on the reaction products between SiO_2 and Li. Amorphous SiO_2 reacts with Li in a two-step reaction process with the following (equations (1–3)) possible mechanisms [24],

$$5SiO_2 + 4Li^+ + 4e^- \longleftrightarrow 2Li_2Si_2O_5 + Si \quad (1a)$$

$$5Si + 22Li^+ + 22e^- \longleftrightarrow Li_{22}Si_5 \quad (1b)$$

$$2SiO_2 + 4Li^+ + 4e^- \rightarrow Li_4SiO_4 + Si \quad (2a)$$

$$5Si + 22Li^+ + 22e^- \longleftrightarrow Li_{22}Si_5 \quad (2b)$$

$$SiO_2 + 4Li^+ + 4e^- \rightarrow 2Li_2O + Si \quad (3a)$$

$$5Si + 22Li^+ + 22e^- \longleftrightarrow Li_{22}Si_5 \quad (3b)$$

Lithium metal initially reacts with SiO_2 to produce lithium silicates ($Li_2Si_2O_5$ and Li_4SiO_4), lithium oxide (Li_2O), and Si; the Si produced in the first step then reacts with Li to produce lithiated Si. According to Yan et al., [24], reaction 1 (equations (1a) and (1b)) alone results in a theoretical reversible capacity of 749 mAh/g, reaction 2 (equations (2a) and (2b)) alone results in 980 mAh/g, and reaction 3 (i.e., equations (3a) and (3b)) alone results in 1961 mAh/g. Depending on the sample configuration (nanoparticle, nanotube, or thin film); electrochemical conditions (charge rates, potentials, or potential sweep rate); and type of materials in contact (electrolyte and constituents of composite electrode), either one reaction, a combination of two concurrent reactions, or all possible reaction mechanisms occur simultaneously in SiO_2 samples during lithiation/delithiation. Further, (equation (1)) shows reversible reaction, and (equations (2) and (3)) show irreversible reactions. For example, Sun et al. [19] cycled thin-film SiO_2 and found $Li_2Si_2O_5$ and Li_xSi phases in their sample at the end of lithiation. They were able to cycle the films reversibly with stable capacities of ~500 mAh/g, suggesting that the $Li_2Si_2O_5$ reaction is reversible; this was also confirmed by several other studies [13, 20, 24]. Conversely, Zhang et al. [17], Favors et al. [22], Phillippe et al. [25], and Guo et al. [23], observed that their samples only contained Li_4SiO_4 and Li_2O products with Li_xSi phase undetectable in some cases, and found that these two reactions are irreversible; hence, the lithium consumed to form these products is not recoverable after formation. Yan et al. [24] cycled hollow porous SiO_2 nanocubes and observed all three products ($Li_2Si_2O_5$, Li_4SiO_4, and Li_2O) in their sample. Therefore, the capacity of the SiO_2 anode depends on the number and type of (equations (1–3)) reactions taking place in the sample. Nevertheless, some or all of these possible reactions lead to significantly higher capacities compared to the capacity of graphite which is 372 mAh/g.

Although the material design efforts [13–16] resulted in innovative core-shell microstructures and the characterization studies [19–24] helped in understanding electrochemical and structural change behavior of lithiated SiO_2 products, many key questions pertaining to their mechanical behavior remain unanswered. For example, are the reaction products between Li and SiO_2 stronger than lithiated Si? Will the strength of

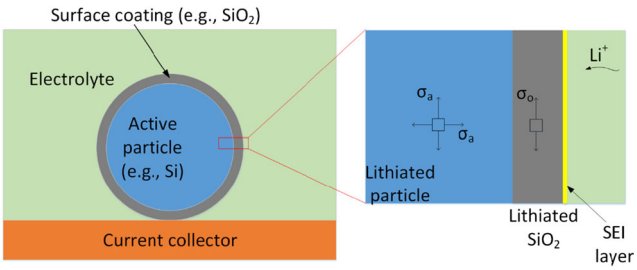

Fig. 1 Schematic of an active particle (Si) with oxide coating. The zoomed view shows that volume expansion of Si due to lithiation induces stresses in the, Si particle, SiO_2 coating, and SEI. Also, the oxide layer isolates the active particle from the electrolyte producing a stable SEI layer

lithiated SiO_2 change during electrochemical cycling? What level of stresses are generated in the SiO_2 coating during electrochemical cycling? Also, the above studies on coated electrodes provide qualitative understanding only and do not provide quantitative understanding. Several studies [26–31] reported that the mechanical properties of electrode materials (both anodes and cathodes) change during electrochemical cycling; and similarly, the properties of SiO_2 may change continuously during the lithiation/delithiation process due to the formation and decomposition of reaction products in (equations (1–3)). This knowledge is necessary to develop durable Si/SiO_2 core shell structures or just SiO_2-based electrodes. For example, note, from Fig. 1, that the oxide layer (or shell) should be able to sustain the deformation and stress levels imposed by the volume expansion of active (core) materials (which could be 300% for Si) to be successful in promoting SEI stability and mechanical integrity for the long cyclic-life operation of the oxide-coated battery electrodes. Despite the importance, no experimental study exists on the mechanical properties or stress measurement of the lithiated silicon dioxide. Due to the lack of experimental data on the mechanical properties of lithiated SiO_2, existing studies model the coating as simple linear elastic or elastic-plastic material with estimated properties.

Hence, the primary objective of this study is to measure the magnitude of stresses generated in SiO_2 material, understand how these stresses vary during electrochemical cycling, and further, understand how the variation of mechanical properties affect the mechanics of core-shell type of particles. To this end, real-time stress evolution in SiO_2 thin films was measured during lithiation/delithiation cycling using substrate curvature method. A simple finite element model of a Si nanotube coated with a thin layer of SiO_2 was developed using the material properties measured from the experiments. The hollow nanotube developed in the FE model was then lithiated/delithiated to see how the stresses would evolve in the particles when experimentally measured mechanical properties of lithiated oxide layer were used as opposed to a simple elastic-plastic assumption. This study provides basic mechanical properties and an understanding of mechanics that will help in the design of high-energy-density and durable SiO_2-based electrode microstructures.

Experimental Methods

Electrode Fabrication and Electrochemical Cell Assembly

Electrode samples were prepared by depositing thin films of Ti (~5 nm, as adhesive layer), Fe (~200 nm, as current collector), and a 100 nm amorphous SiO_2 (or a-SiO_2) on a double-side polished fused silica substrate (50.8 mm diameter and ~500 μm thickness); (Fig. 2(a)) inset shows the details of the films. The Ti and Fe films were deposited using DC sputtering whereas SiO_2 film was deposited using RF sputtering technique. The deposition rate of SiO_2 film was 1 nm per minute. Process pressure during the deposition of all these films was maintained at 3 mTorr. The substrate platen on which the samples were mounted was rotated at 20 RPM during the deposition process to minimize the variation of film thickness. The planar thin film geometry used in this study eliminates the effect of binders and other additives of a composite electrode, and it allows for an accurate characterization of mechanical and electrochemical behavior of SiO_2. Hence, the thin film on substrate samples is ideal to study the fundamental mechanical behavior of electrodes.

A homemade electrochemical beaker cell was assembled in an argon filled glovebox (MBraun Inc., maintained at 25 °C with less than 0.1 ppm of O_2 and H_2O) by using the deposited SiO_2 film on elastic substrate (sample details can be seen in the (Fig. 2(a)) inset) as a working electrode and a 1.5 mm thin lithium foil as a counter/reference electrode. A polymer separator (Celgard Inc.) was used to prevent physical contact between electrodes, and a 1 M $LiPF_6$ in a 1:1:1 ratio (wt%) of ethylene carbonate (EC): diethyl carbonate (DEC): dimethyl carbonate (DMC) was used as the electrolyte. The casing of the cell was made from Teflon, the cap of the cell was made from stainless steel; the cap has a glass window which enables optical access to the sample for substrate curvature measurements using laser setup show in (Fig. 2(a)).

Electrochemical Measurements

The amorphous SiO_2 films were lithiated and de-lithiated under a galvanostatic, i.e., constant, current density of $i \sim 2\ \mu A/cm^2$, conditions between 3 V and 0.01 V vs. Li/Li^+ using Solartron 1470 E potentiostat; the stress and potential response of the sample were recorded during this process. This current density was chosen to avoid any concentration (or stress) gradients within the SiO_2 thin film during electrochemical cycling. Some cells were interrupted after the first lithiation process and after the subsequent delithiation process; a portion of the electrode sample was separated each time while the remaining portion of the electrode was cycled further. The harvested samples were then soaked for 5 min and rinsed in dimethyl carbonate, then transported in to the SEM chamber for analysis. Care was taken to minimize the exposure of samples to ambient atmosphere during the transfer. This SEM analysis was carried out to ascertain if the SiO_2 films developed any cracks and if so, when they occurred.

Stress Measurement Using MOS Setup

Stress evolution in an a-SiO_2 electrode during lithiation/delithiation cycling was measured by monitoring the changes

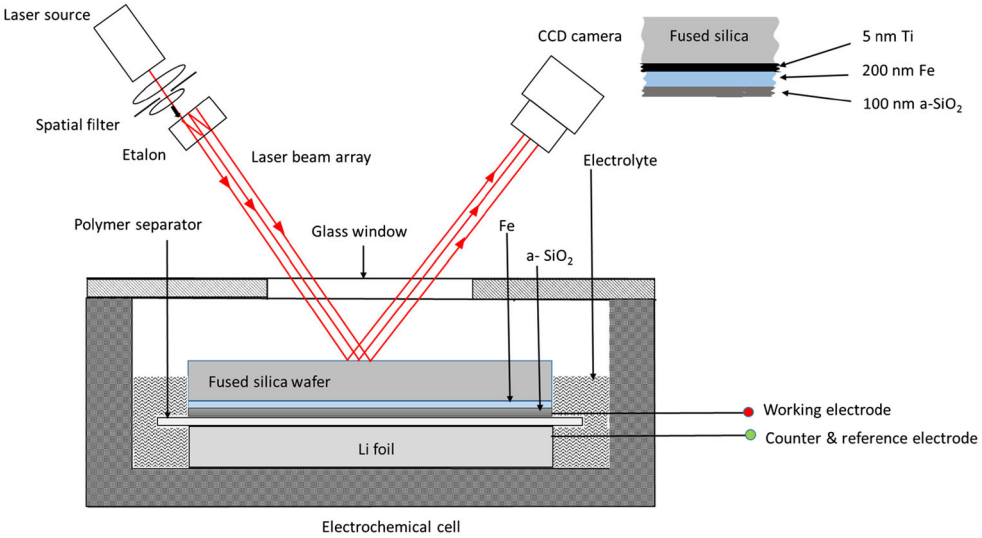

(a)

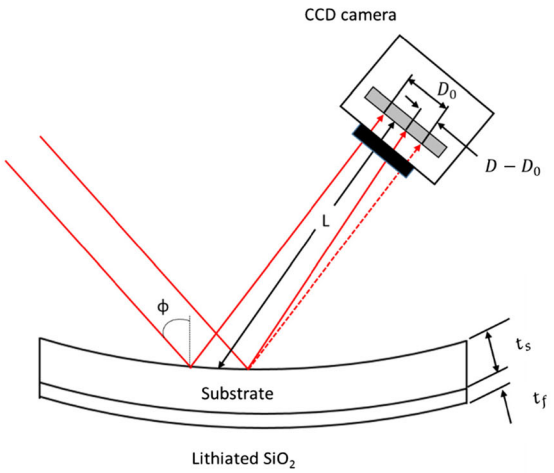

(b)

Fig. 2 Electrochemical cell with MOS set up for stress measurement is shown in (**a**) and various relevant optical parameters are defined in (**b**)

in the curvature of fused silica substrate with the help of a multi-beam optical sensor (MOS) setup (k-Space Associates, Dexter, MI), illustrated in (Fig. 2(a)). The MOS setup has a laser source which produces a single collimated beam and two etalons that were arranged to generate a 2 × 2 array of laser beams. The array of beams reflected from the sample surface (Fig. 2(a)) is captured by a CCD camera, and appears as a 2 × 2 array of circular dots (cross section of the laser beams) on a computer monitor. The sample curvature could be determined by measuring the relative displacement of the center of these laser spots as,

$$\kappa = \frac{cos\emptyset}{2L}\left\{\frac{D-D_o}{D_o}\right\} \tag{4}$$

where D is the distance between the center of laser spots, D_o is the initial distance, $\emptyset$ is the angle of the laser beam as defined in (Fig. 2(b)), and L is the optical path length as shown in (Fig. 2(b)). The factor $cos\ \emptyset/2L$ is known as the mirror constant, which is specific to a given setup; hence, it is obtained by calibrating the system with a mirror of known curvature. The 2 × 2 array of the laser spots enables curvature measurement in two orthogonal directions. Note, from (Fig. 2(a)), that although the Li foil, separator, and SiO_2 films were submerged in the electrolyte, the surface of the elastic substrate from which the laser beams were reflected was not submerged. This was done to prevent the complexities associated with the laser beams going through the electrolyte.

The biaxial stresses in the SiO_2 film are related to the substrate curvature by Stoney's equation [32]

$$\sigma = \frac{E_s t_s^2 k}{6 t_f (1-\upsilon_s)} \tag{5}$$

Where E_s is Young's modulus of the substrate and t_s is the thickness of the substrate, υ_s is Poisson's ratio of substrate, and t_f is the thickness of the SiO_2 film. The film thickness t_f in (equation (5)) will evolve continuously during the experiment due to the chemical reaction between SiO_2 and Li. Although there are no direct, well-controlled experiments on thickness evolution measurements of lithiated SiO_2, first-order estimates can be made. It was observed from a TEM analysis that lithiation of SiO_2 may result in a volumetric strain of 230% [17]; similarly, Li reaction with SiO results in a volume expansion of 200% [21]. Further, Zhang et al. [17] showed, from DFT and MD calculations, that the volume (or film thickness in the current samples) of lithiated SiO_2 increases linearly with the state of charge. Hence, though the volume expansion depends on the type of reactions that are occurring in the film, it is reasonable to assume that SiO_2 expands linearly during lithiation as per (equation (6)),

$$t_f = t_f^0(1+2z) \tag{6}$$

Here t_f^0 is initial film thickness and z is state of charge (SOC) which changes between 0 and 1; z = 1 indicates a capacity of 749 mAh/g and a volumetric strain of 2.

Finite Element Model

Figure 3(a) shows the schematic of an amorphous silicon nanotube (internal and external radii of 140 nm and 160 nm, respectively) with a uniform SiO_2 coating of 10 nm thickness considered for simulation; although these dimensions were selected based on typical Si/SiO_2 nanotube dimensions published in the literature [13, 33], the model is more general and the observations are applicable to other particle dimensions. The finite element package Abaqus [34] was used to simulate the lithiation/delithiation process of the Si nanotube coated with SiO_2.

Figure 3(b) shows the finite element mesh of the Si nanotube coated with SiO_2, which contains 7380 linear plain strain elements and 7656 nodes, with appropriate boundary conditions. The interface between Si and SiO_2 is assumed to be perfectly bonded. To maintain focus on the mechanics, the solid electrolyte interface formation on the electrode particle was ignored, and a simple model for Li diffusion according to (equations (7) and (8)) was adopted, where the flux J is driven by the concentration gradient only, i.e., diffusion stress coupling is ignored [35, 36].

$$\frac{\partial \overline{C}}{\partial t} = -\nabla . \boldsymbol{J} \tag{7}$$

$$\boldsymbol{J} = -\boldsymbol{D}\nabla \overline{C} \tag{8}$$

A fully lithiated Si core and SiO_2 coating have a normalized lithium concentration of $\overline{C}_{Si} = 1$ (corresponding to 3579 mAh/g) and $\overline{C}_{SiO_2} = 1$ (corresponding to 749 mAh/g), respectively; whereas $\overline{C}_{Si} = 0$ is pure Si *and* $\overline{C}_{SiO_2} = 0$ is pure SiO_2. A constant diffusion coefficient of $D = 10^{-11}$ m^2/s [37] and $D = 10^{-19}$ m^2/s [38] was used for lithium diffusivity in SiO_2 and Si, respectively. An analogous heat-transfer and thermal expansion framework available in Abaqus was used to model the diffusion of lithium and the associated volume expansion of SiO_2 and Si, where temperature is assumed to be the Li concentration; An equivalent thermal expansion coefficient alpha as a function of Li concentration is defined as

$$\alpha_{Si} = \frac{\ln\left(1+2.7\overline{C}_{Si}\right)}{3\overline{C}_{Si}} \tag{9}$$

$$\alpha_{SiO_2} = \frac{\ln\left(1+2\overline{C}_{SiO_2}\right)}{3\overline{C}_{SiO_2}} \tag{10}$$

to induce a 270% increase in volume of Si and 200% volume increase of SiO_2 at full lithiation. The normalized lithium

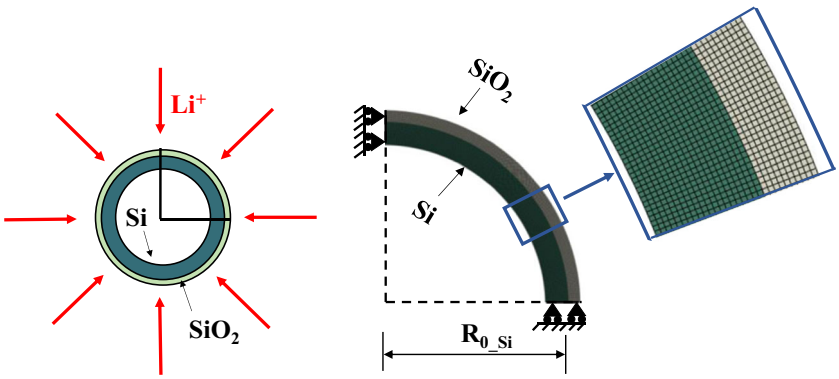

Fig. 3 Schematic of Si nanotube coated with SiO_2 is shown in (**a**) and the plane strain finite element mesh (quarter of model due to symmetry) along with symmetry boundary conditions are shown in (**b**)

concentration was prescribed directly on the surface of the SiO_2 coating, which was varied from 0 to 1 as a function of time to get 1C rate of lithiation/delithiation of Si core.

The plastic deformation behavior of lithiated Si is modeled with standard von-Mises plasticity with lithium concentration dependent mechanical properties such as Young's modulus, Poisson's ratio, and flow stress as per [39, 40]. Consequently, a linear relation was used to calculate Young's modulus, Poisson's ratio, and flow stress of Si at any given state of charge (SOC) as.

$$E_{\overline{C}} = E_{Si} + \overline{C}_{Si}(E_{Li_{4.4}Si} - E_{Si}) \tag{11}$$

$$\nu_{\overline{C}} = \nu_{Si} + \overline{C}(\nu_{Li_{4.4}Si} - \nu_{Si}) \tag{12}$$

$$\sigma_{y\overline{C}} = \sigma_{ySi} + \overline{C}\left(\sigma_{yLi_{4.4}Si} - \sigma_{ySi}\right) \tag{13}$$

Where E_{Si} = 150 GPa, σ_{ySi} = 1.5 GPa, and ν_{Si}= 0.21 are modulus, yield stress, and Poisson's ratio of pure Si respectively, and $E_{Li_{4.4}Si}$ = 50 GPa, $\sigma_{yLi_{4.4}Si}$ = 0.6 GPa and $\nu_{Li_{4.4}Si}$ = 0.23 are properties of fully lithiated Si as shown in [40] [39]. Young's modulus and Poisson's ratio for SiO_2 were taken as constant (E = 90 GPa, ν = 0.17) [14].

Three different simulations were carried out: 1) a bare Si nanotube was lithiated and delithiated without SiO_2 coating to get the baseline behavior, 2) SiO_2 coating was treated as an elastic-plastic mechanical constraint layer (with σ_y = 2.52 GPa [14]) that allows lithium-ions to pass through but doesn't react or undergo volume expansion (i.e., $\alpha_{SiO_2} = 0$), and 3) a SiO_2 coating was treated as elastic-perfectly plastic material where concentration-dependent yield stress was obtained from the in-situ stress experiments explained in the previous section, and the SiO_2 coating expands as per (equations (8) and (10)).

Results and Discussion

Electrochemical and Mechanical Behavior of SiO_2 Film during Lithiation/Delithiation Cycling

Figure 4(a) shows SiO_2 electrode potential as a function of electrode capacity during electrochemical cycling under galvanostatic conditions (i.e., constant i = 2 μA/cm^2 corresponding to C/9 rate). The open circuit potential of pristine (or as prepared) SiO_2 film was about 3.0 V vs. Li/Li$^+$, and upon lithiation it drops rapidly to approximately 1.6 V vs. Li/Li$^+$ where a small pseudo plateau was observed. This plateau was nonexistent in the remaining cycles and occurred at a potential higher than the electrolyte decomposition potentials; hence, this could be attributed to an irreversible reaction between SiO_2 and Li which was also reported in earlier studies

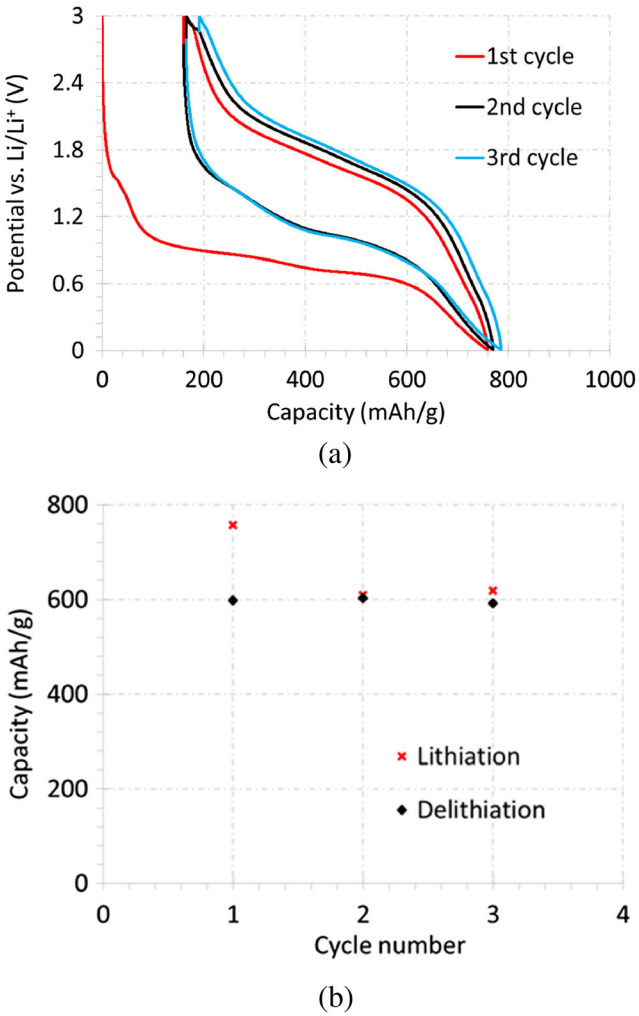

Fig. 4 (**a**) SiO_2 electrode potential as a function of its specific capacity during galvanostatic lithiation/de-lithiation cycling at C/9 rate and (**b**) shows lithiation/delithiation capacities as a function of cycle number

[24, 41]. With further lithiation, the potential rapidly drops again from 1.6 to 1.0 V vs. Li/Li$^+$ and thereafter decreases gradually (almost linearly) to 0.6 V vs. Li/Li$^+$ at 600 mAh/g. As the potential in this linearly decreasing region is higher than the lithiation potential of Si (which is below 0.4 V vs. Li/Li$^+$), most of the lithiation in this region probably leads to the formation of lithium silicates, lithium oxides, and Si: i.e., only the first step in the reactions showed in (equations (1–3)). Beyond 0.6 V vs. Li/Li$^+$ the potential decreases rapidly to 0.01 V vs. Li/Li$^+$, leading to a total first-cycle lithiation capacity of 760 mAh/g. The second reaction step between Li and pure Si shown in (equations (1–3)) occurs at potentials below 0.4 V vs. Li/Li$^+$; note from (Fig. 4(a)) that the capacity corresponding to these reactions (where Si could have reacted with Li) is merely ~100 mAh/g. Hence, it can be assumed that the amount of Si produced during the lithiation of SiO_2 thin films and the associated volume changes may be negligible compared to the contribution from the other products in (equations (1–3)). Upon delithiation, the potential increases quickly to

1.2 V vs. Li/Li^+ within a capacity change of 120 mAh/g, followed by a gradual increase until 2.0 V vs. Li/Li^+ is reached at 240 mAh/g, and a sharp rise to 3 V vs. Li/Li^+ thereafter.

The potential response of the SiO_2 film during the first lithiation process is significantly different from that of subsequent lithiation cycles. This could be due to a combination of factors, such as SEI formation, and irreversible chemical reactions (equations (2a) and (3a)) that mainly occur in the first cycle. In other words, the film in the second cycle is not the same as the pristine SiO_2 film and contains some irreversible reactions products, such as Li_4SiO_4 and Li_2O; this is reflected in the differences in the electrode potentials of first and second lithiation processes. Due to the irreversible reactions, such as the formation of lithium silicates, Li_2O, SEI, and possible entrapment of Li, there will be some capacity loss during the cycling process, and it will be severe in the first cycle. For example, note from (Fig. 4(b)) that the first cycle lithiation capacity of SiO_2 film is 760 mAh/g and the delithiation capacity is 600 mAh/g: i.e., a loss of about 160 mAh/g at a coulombic efficiency of 78%. The coulombic efficiency quickly increases to 99% (i.e., negligible loss) from the second cycle with a stable delithiation capacity of 600 mAh/g as shown in (Fig. 4(b)). It can be assumed that this 600 mAh/g of reversible capacity is mainly due to the reversible reaction shown in (equation (1)) (i.e., formation/decomposition of Li_2SiO_5) and not due to formation of lithiated Si. This is because the potentials at which these reactions are occurring are clearly above 0.4 V vs. Li/Li^+, where Li may not react with Si (hence cannot contribute to the capacity).

Unlike the crystalline Si, volume expansion of lithiated SiO_2 seems to be uniform and isotropic. Figure 5(a) shows that the substrate curvature (which is proportional to stress times film thickness according to (equation (5)) as a function of time during electrochemical cycling plotted in two directions orthogonal to each other is almost same. This was consistent in all the samples tested here; also, the curvature values are consistent among several samples (see Fig. 5(b)), suggesting that the film expansion was isotropic and uniform.

Figure 6(b) shows the stress in SiO_2 film as a function of capacity during lithiation/delithiation cycling; this is the true stress in the film, calculated based on the stress-thickness data (shown in Fig. 6(a)), which is obtained directly from the experiments, and the film thickness, which is calculated from (equation (6)). Note that the SiO_2 film is subjected to compressive stresses upon lithiation. This is because when the SiO_2 film is lithiated (i.e., lithium insertion into SiO_2 film), the film expands in the thickness direction, i.e., in the direction normal to the plane of the substrate; however, the substrate constrains the in-plane expansion which induces equi-biaxial in-plane compressive stress field in the film. As the lithiation progresses, the compressive stress increases initially with capacity, reaches a peak value of 3.1 GPa at 450 mAh/g, and thereafter decreases to 2.4 GPa at 756 mAh/g. These stress

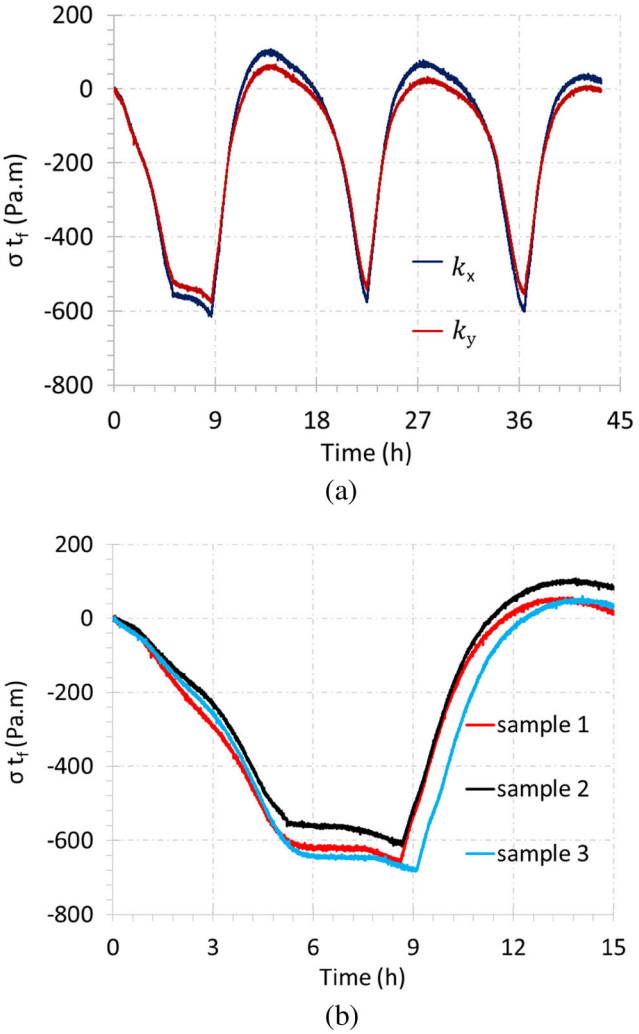

Fig. 5 Variation of stress-thickness value (which is proportional to substrate curvature) as a function of time is plotted (**a**) for two different directions (orthogonal to each other) in a single sample and (**b**) for three different samples

values are significantly higher compared to the tensile strength of pure SiO_2 films (fabricated by PECVD method such as the ones in this study) which is only ~ 0.6 GPa to 1 GPa [42]. Note from (Fig. 6(b)) that the stress increases linearly at low Li concentrations: i.e., below 70 mAh/g capacity and 0.4 GPa of stress, which could be a linear elastic response of the film. Although the pure SiO_2 is brittle, the lithiated SiO_2 seems to be undergoing extensive inelastic deformation as the stress response beyond 70 mAh/g and 0.4 GPa is non-linear. This suggests that addition of Li to SiO_2 film not only strengthens the film, as it is able to sustain stress values as high as 3.1 GPa, but also makes SiO_2 ductile so that it can sustain large deformation without fracture. To confirm that the films are intact even after subjecting them to this level (i.e., 3.1 GPa) of stress, SEM analysis was carried out on the samples at different intervals during cycling. Figure 7(a), (b), and (c) show the SEM images of the samples in pristine condition, after first lithiation

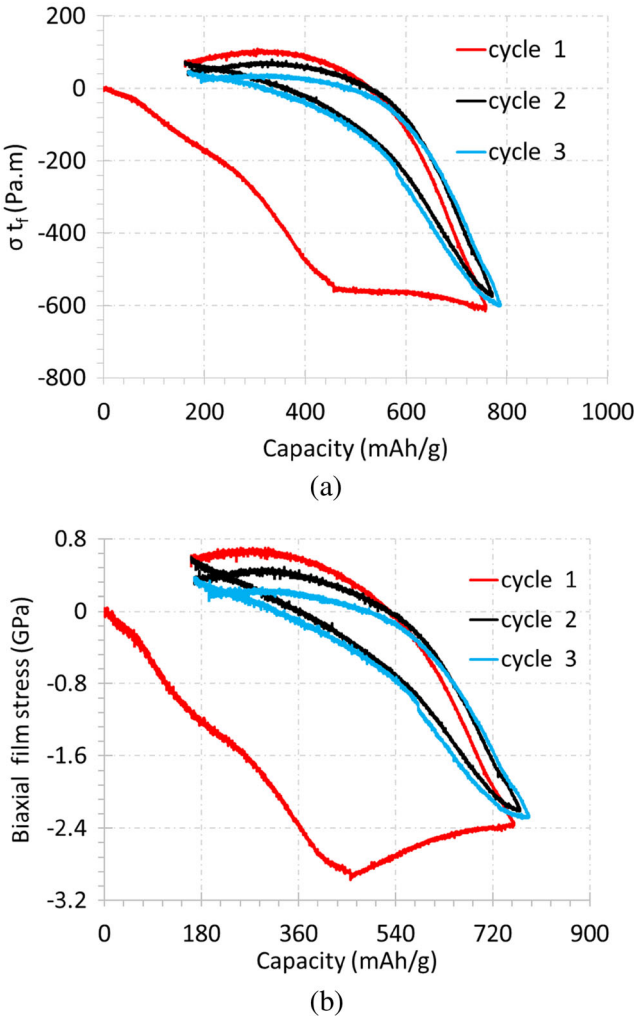

Fig. 6 Stress-thickness value (or substrate curvature) and biaxial stress in SiO_2 film as a function of specific capacity during galvanostatic lithiation/delithiation at C/9 rate is plotted in (**a**) and (**b**), respectively

and first delithiation respectively. Note that, although there are some morphological changes, the film did not crack during the first lithiation process. This could be attributed to two things: (1) the compressive nature of stress tends to suppress cracking and (2) the lithiated SiO_2 products are tougher than the pure SiO_2. Before performing any electrochemistry, the residual stresses in the SiO_2 films were measured by recording the curvature changes of the substrate before and after SiO_2 deposition. It was observed that the residual stress was only ~80 MPa, which was insignificant compared to the lithiation-induced stress and hence, not included in the plots.

Upon delithiation (i.e., as the Li is removed from SiO_2) the stresses quickly change towards tensile direction. They reach a peak value of approximately 0.7 GPa and decrease with further delithiation. The stress response of the film in the first cycle is completely different from that of the subsequent cycles. This could be due to a combination of different factors such as irreversible reactions (including SEI layer formation), that occur in the first cycle but are absent in the subsequent cycles, and film cracking (which is evident from the SEM images) after first delithiation. The shrinking of the stress-capacity loop and decreasing peak stress also confirm that the film is cracking after the first cycle. However, it was reported, e.g., [14] that SiO_2 coatings on Si nanotubes cycled without damage for a few hundred cycles. This can be attributed to the thickness of the films, which is below 20 nm in [14] but 100 nm in this study; in general, thicker films have a higher propensity for cracking [43]. Hence, 100 nm may not be an ideal coating thickness for electrode particles. However, due to size-dependent fracture behavior, sufficiently thin SiO_2 films could sustain stresses as high as 3.1 GPa. It should be noted that although the data presented here provides valuable information that will help in developing electro-chemo-mechanics constitutive models for SiO_2, an in-situ XRD measurement, which is beyond the scope of this work, is necessary to provide a thorough understanding of the SiO_2 mechanical behavior and provides complimentary data to the measured stress data.

Effect of SiO_2 Mechanical Properties on the Deformation Behavior of Core-Shell Particles

Although reports such as [14, 41] showed that SiO_2 coatings on Si particles improved their cyclic performance, one of the obvious questions that remains to be answered is how a brittle coating like SiO_2 sustained a 300% volume expansion imposed by Si without cracking? The stress measurements and observations made in the previous section provide some clues; i.e., the lithiated SiO_2 products are stronger than pure SiO_2, and they undergo extensive plastic deformation, which generally leads to increased toughness [43]. However, knowledge

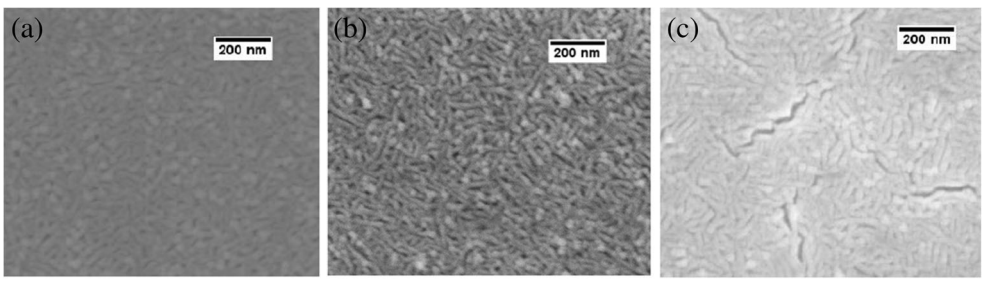

Fig. 7 Scanning electron microscope images of (**a**) pristine SiO_2 film, (**b**) SiO_2 film after first lithiation, and (**c**) SiO_2 film after first delithiation. No cracking occurred in the first lithiation process but film starts cracking after first delithiation

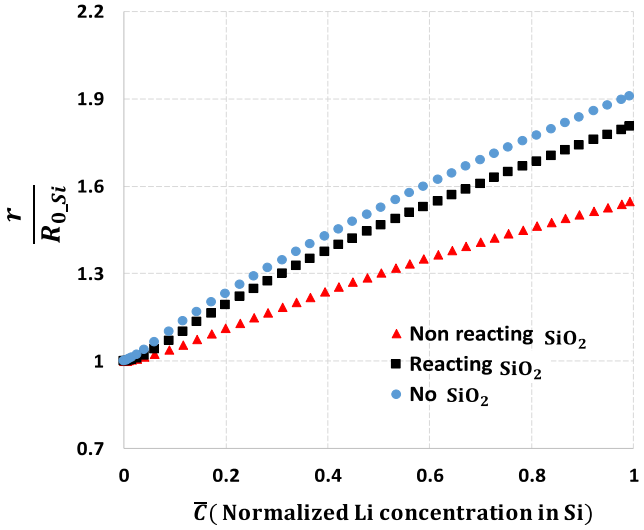

Fig. 8 Evolution of normalized radial displacement at the outer surface of Si nanotube as a function of Li concentration during lithiation for 3 different cases: (i) filled circles represent the baseline expansion behavior of Si nanotube without SiO_2 coating, (ii) filled triangles represent a case where SiO_2 coating was modeled as elastic-plastic mechanical constraint layer which allows Li^+ to diffuse (such as an artificial SEI), and (iii) filled squares represent a case where SiO_2 was modeled as per the measured stress response from section 4.1

of the displacement and stress distribution in SiO_2 coatings on Si nanoparticles/nanotubes during electrochemical cycling will provide a more complete picture of how coatings survived hundreds of cycles.

Figure 8 shows expansion behavior (normalized radius value at the outer surface) of the Si nanotube as a function of lithium concentration during electrochemical lithiation for three different simulation conditions. As expected, the expansion of bare Si (i.e., filled circles) is the largest at any given lithium concentration, with a final radius to original radius ratio of 1.9 at the end of lithiation. However, the Si nanotube expanded only 1.5 times the original dimension when the SiO_2 layer was modelled as a mechanical clamping layer and expands approximately 1.8 times when the SiO_2 layer was modeled with the measured stress data (concentration dependent yield stress, (Fig. 6(b))). This shows that SiO_2 does provide some clamping effects but the constraint may not be as strong as reported earlier, and the assumption that clamping effect induced by SiO_2 coating promotes mechanical stability of SEI layer needs further investigation.

Figure 9(a), (b) show hoop stress contours of the Si nanotube coated with SiO_2 at the end of lithiation for two different cases: (i) SiO_2 coating was modeled with the measured stress

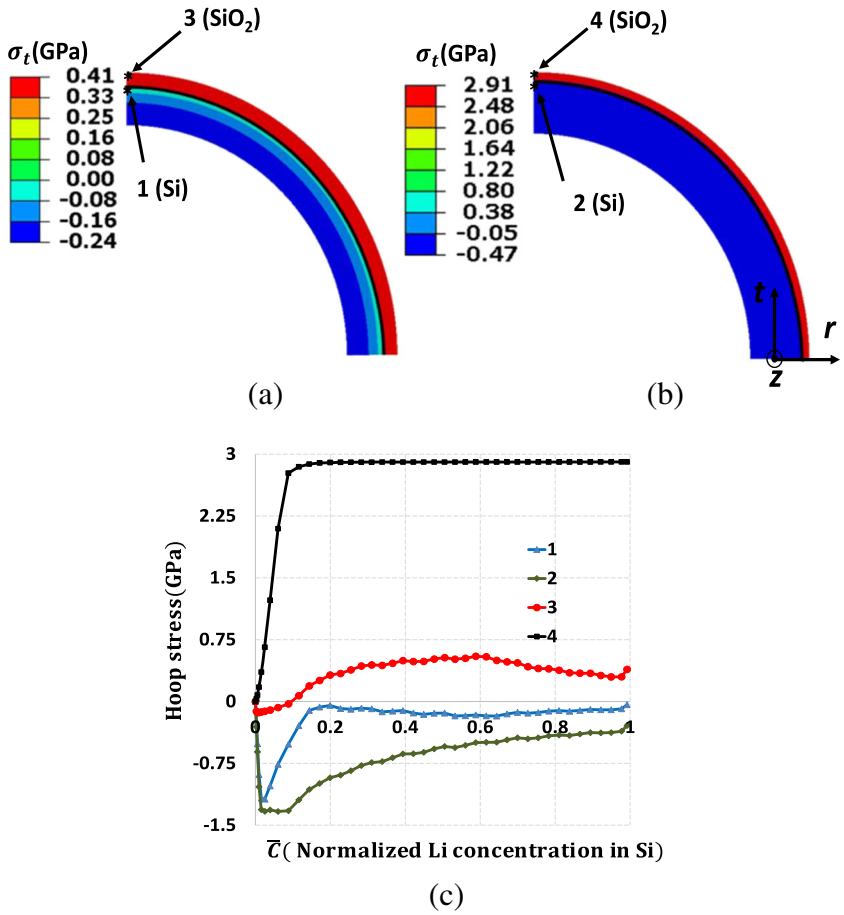

Fig. 9 Contours of hoop (or circumferential) stress component at the end of lithiation in Si nanotube coated with SiO_2 (**a**) when SiO_2 coating was modeled as per the measurements in section 4.1 and (**b**) when SiO_2 modelled as elastic-perfectly plastic mechanical constraint layer. (**c**) depicts the stress evolution at the outer surface of Si and at the outer surface of SiO_2 coating for the (**a**) and (**b**) cases

data (ii) SiO_2 coating was modelled as a mechanical constraint layer. It can be observed that when SiO_2 coating is assumed as a pure mechanical clamping layer with elastic-plastic properties [13], the hoop stress in SiO_2 reaches as high as 2.9 GPa, which is significantly higher tensile stress than the fracture strength of SiO_2, which could lead to cracking. However, when SiO_2 is modeled using the measured stress response, the peak stress in SiO_2 at any stage of lithiation (see Fig. 9(c)) is less than 0.41 GPa, which is lower than the fracture strength of SiO_2. This clearly provides a plausible explanation as to why the coatings reported in earlier studies [14, 41] were able to sustain a 300% volume change of Si for several cycles. Further, the stresses in Si particles are also relatively less when measured properties of SiO_2 are used in the model. In addition to the inelastic nature of lithiated SiO_2 and stronger lithiated products as mentioned earlier, these FE results show that the lower hoop stresses in SiO_2 and Si were probably the reason for superior performance of Si/SiO_2 nanotubes in [14, 41]. Therefore, it is important to incorporate the measured electrochemical and stresses response while developing electro-chemo-mechanics models of SiO_2, which will be used to design complex SiO_2 coated Si electrode architectures.

Conclusions

Real-time stress evolution in planar SiO_2 thin film electrodes were measured while cycling against Li foil counter/reference electrodes under galvanostatic lithiation/delithiation cycling. It was observed that upon lithiation the SiO_2 film undergoes compressive stress which increases linearly at low Li concentrations, below 70 mAh/g capacity and 0.4 GPa of stress, possibly representing a linear elastic response of the film. Upon further lithiation the electrode undergoes extensive plastic deformation with a peak compressive stress of 3.1 GPa at 450 mAh/g and thereafter decreases to 2.4 GPa at 756 mAh/g at the end of lithiation. Upon delithiation the stress quickly changes towards tensile direction and reaches a peak value of approximately 0.7 GPa. The first-cycle coulombic efficiency of the film was 78% which increases to 99% in the second cycle; in addition, potential and stress response of the film in the first lithiation process was significantly different from the subsequent cycles. This behavior along with the large first cycle loss was attributed to SEI formation and irreversible chemical reactions between SiO_2 and Li. Further, SEM analysis of the sample showed that the film was intact in the first cycle but started cracking after that. This premature cracking of SiO_2 in this study, as opposed to the coatings in earlier reports, which cycled without cracking for several hundred cycles, was attributed to relatively thick films in the current study, which tend to have a larger crack-driving force.

To be able to provide mechanistic explanation as to how highly brittle SiO_2 coatings on Si were able improve the cyclic performance of Si [14, 41] by sustaining 300% volume expansion for several hundred cycles, a simple finite element model of SiO_2-coated Si nanotube (core-shell type microstructure) was developed; the SiO_2 coating was modeled using measured stress and electrochemical response. It was observed that the clamping action provided by SiO_2 is relatively lower than was reported in the literature, which suggests that the current understanding of clamping effects of oxide coatings providing stable SEI needs to be investigated further. Also, it was observed that the maximum stress in the SiO_2 coating during electrochemical cycling (i.e., under 300% volume change of Si) is approximately 0.41 GPa, which is less than the fracture strength of pure SiO_2 films, providing a plausible explanation as to why oxide coatings survived several hundreds of cycles without failure.

This observation along with the stress measurements suggests that the addition of Li to SiO_2 film not only strengthens the film, as they are able to sustain stress values as high as 3.1 GPa, but also makes it ductile so that it can sustain large deformation without fracture. In addition to the above insights, the results and observations made in this study are also useful (i) to develop a comprehensive electro-chemo-mechanics models of SiO_2 films and (ii) to design and develop next generation SiO_2 coating-based core-shell type of microstructures for electrodes that are mechanically and chemically stable. Finally, the battery electrodes based on Si will have a thin layer of native oxide film on all the particles, and it is important to understand the electrochemical and mechanical properties of the oxide layer for which a basic preliminary understanding was given in this study.

Acknowledgements Authors would gratefully acknowledge funding from the National Science Foundation through the grant no NSF-CMMI-1652409 and from the New Jersey Institute of Technology through faculty seed grant 2016.

References

1. Kasavajjula U, Wang C, Appleby AJ (2007) Nano- and bulk-silicon-based insertion anodes for lithium-ion secondary cells. J Power Sources 163:1003
2. Besenhard JO, Yang J, Winter M (1997) Will advanced lithium-alloy anodes have a chance in lithium-ion batteries? J Power Sources 68:87
3. Beaulieu LY, Eberman KW, Turner RL, Krause LJ, Dahn JR (2001) Colossal reversible volume changes in lithium alloys. Electrochem Solid State Lett 4:A137
4. Beaulieu LY, Hatchard TD, Bonakdarpour A, Fleischaue MD, Dahn JR (2003) Reaction of li with alloy thin films studied by *in situ* AFM. J Electrochem Soc 150:A1457
5. Aurbach D (2000) Review of selected electrode–solution interactions which determine the performance of li and li ion batteries. J Power Sources 89:206
6. Aurbach D, Moshkovich M, Cohen Y, Schechter A (1999) Study of surface film formation on noble-metal electrodes in alkyl

carbonates/li salt solutions, using simultaneous in situ AFM, EQCM, FTIR, and EIS. Langmuir 15:2947
7. Peled E (1979) Electrochemical behavior of alkali and alkaline earth metals in nonaqueous battery systems - the solid electrolyte interphase model. J Electrochem Soc 126(12):2047
8. Besenhard JO, Winter M, Yang J, Biberacher W (1995) Filming mechanism of lithium-carbon anodes in organic and inorganic electrolytes. J Power Sources 54:228
9. Nadimpalli SPV, Sethuraman VA, Dhalavi S, Lucht B, Chon MJ, Shenoy VB, Guduru PR (2012) Quantifying capacity loss due to solid-electrolyte-interphase layer formation on silicon negative electrodes in Lithium-ion batteries. J Power Sources 215:145
10. Kostecki R, McLarnon F (2003) Microprobe study of the effect of li intercalation on the structure of graphite. J Power Sources 119-121: 550
11. Vetter J, Novák P, Wagner MR, Veit C, Möller K-C, Besenhard JO, Winter M, Wohlfahrt-Mehrens M, Vogler C, Hammoushe A (2005) Ageing mechanisms in lithium-ion batteries. J Power Sources 147: 269
12. Lee YM, Lee JY, Shim H, Lee JK, Park J (2007) SEI layer formation on amorphous Si thin electrode during precycling. J Electrochem Soc 154:A515
13. McDowell MT, Lee SW, Ryu I, Wu H, Nix WD, Choi JW, Cui Y (2011) Novel size and surface oxide effects in silicon nanowires as lithium battery anodes. Nano Lett 11(9):4018
14. Wu H, Chan G, Choi JW, Ryu I, Yao Y, McDowell MT, Lee SW, Jackson A, Yang Y, Hu L, Cui Y (2012) Stable cycling of double-walled silicon nanotube battery anodes through solid–electrolyte interphase control. Nat Nanotechnol 7:310
15. Wu H, Cui Y (2012) Designing nanostructured Si anodes for high energy lithium ion batteries. Nano Today 7:414
16. Wu H, Yu G, Pan L, Liu N, McDowell MT, Bao Z, Cui Y (2013) Stable li-ion battery anodes by in-situ polymerization of conducting hydrogel to conformally coat silicon nanoparticles. Nat Commun 4: 1943
17. Zhang Y, Li Y, Wang Z, Zhao K (2014) Lithiation of SiO2 in li-ion batteries: in situ transmission electron microscopy experiments and theoretical studies. Nano Lett 14:7161
18. Choi S, Jung DS, Choi JW (2014) Scalable fracture-free SiOC glass coating for robust silicon nanoparticle anodes in lithium secondary batteries. Nano Lett 14:7120
19. Sun Q, Zhang B, Fu Z-W (2008) Lithium electrochemisty of SiO_2 thin film electrode for lithium-ion batteries. Appl Surf Sci 254: 3774–3779
20. Chang W-S, Park C-M, Kim J-H, Kim Y-U, Jeong G, Sohn H-J (2012) Quartz (SiO_2): a new energy storage anode material for li-ion batteries. Energy Environ Sci 5:6895–6899
21. Miyachi M, Yamamoto H, Kawai H, Ohta T, Shirakata M (2005) Analysis of SiO anodes for lithium-ion batteries. J Electrochem Soc 152(10):A2089–A2091
22. Favors Z, Wang W, Bay HH, George A, Ozkan M, Ozkan CS (2014) Stable cycling of SiO_2 nanotubes as high-performance anodes for Lithium-ion batteries. Sci Rep 4:4605
23. Guo B, Shu J, Wang Z, Yang H, Shi L, Liu Y, Chen L (2008) Electrochemical reduction of Nano-SiO_2 in hard carbon as anode material for Lithium ion batteries. Electrochem Commun 10:1876–1878
24. Yan N, Wang F, Zhong H, Liu Y, Wang Y, Hu L, Chen Q (2013) Hollow porous SiO_2 Nanocubes towards high-performance anodes for Lithium-ion batteries. Sci Rep 3:1568
25. Philippe B, Dedryvere R, Gorgoi M, Rensmo H, Gonbeau D, Edstrom K (2013) Improved performance of Nanosilicon electrodes using the salt LiFSI: a photoelectron spectroscopy study. J Am Chem Soc 135:9829–9842
26. Nadimpalli SPV, Tripuraneni R, Sethuraman VA (2015) Real-time stress measurements in germanium thin film electrodes during electrochemical Lithiation/Delithiation cycling. J Electrochem Soc 162(4):A2840–A2846
27. Sethuraman VA, Chon MJ, Shimshak M, Srinivasan V, Guduru PR (2010) In situ measurements of stress evolution in silicon thin films during electrochemical Lithiation and Delithiation. J Power Sources 195(15):5062
28. Zhao K, Wang WL, Gregoire J, Pharr M, Suo Z, Vlassak JJ, Kaxiras E (2011) Lithium-assisted plastic deformation of silicon electrodes in lithium-ion batteries: a first-principles theoretical study. Nano Lett 11(7):2962
29. Al-Obeidi A, Kramer D, Thompson CV, Monig R (2015) Mechanical stresses and morphology evolution in germanium thin film electrodes during Lithiation and Delithiation. J Power Sources 297:472–480
30. Boles ST, Sedlmayr A, Kraft O, Monig R (2012) In situ cycling and mechanical testing of silicon nanowire anodes for Lithium-ion battery applications. Appl Phys Lett 100:243901
31. Sheth J, Karan NK, Abraham DP, Nguyen CC, Lucht BL, Sheldon BW, Guduru PR (2016) In situ stress evolution in $Li_{1+x}Mn_2O_4$ thin films during electrochemical cycling in li-ion cells. J Electrochem Soc 163(13):A2524–A2530
32. Freund LB, Suresh S (2004) Thin films materials: stress, defect formation and surface evolution. Cambridge University Press, Cambridge
33. Ryu I, Choi JW, Cui Y, Nix WD (2011) Size-dependent fracture of Si nanowire battery anodes. J Mech Phys Solids 59:1717
34. Abaqus (2016) Abaqus Reference Manuals, Dassault Systèmes Simulia Corp., Providence
35. Zhang X, Shyy W, Sastry AM (2007) Numerical simulation of intercalation-induced stress in li-ion battery electrode particles. J Electrochem Soc 154(10):A910–A916
36. Sethuraman VA, Srinivasan V, Bower AF, Guduru PR (2010) In situ measurements of stress-potential coupling in lithiated silicon. J Electrochem Soc 157(11):A1253–A1261
37. Ostadhossein A, Kim S-Y, Cubuk ED, Qi Y, van Duin AC (2016) Atomic insight into the lithium storage and diffusion mechanism of SiO2/Al2O3 electrodes of lithium ion batteries: ReaxFF reactive force field modeling. J Phys Chem A 120(13):2114–2127
38. Bucci G, Nadimpalli SP, Sethuraman VA, Bower AF, Guduru PR (2014) Measurement and modeling of the mechanical and electrochemical response of amorphous Si thin film electrodes during cyclic lithiation. J Mech Phys Solids 62:276–294
39. Santimetaneedol A, Tripuraneni R, Chester SA, Nadimpalli SP (2016) Time-dependent deformation behavior of polyvinylidene fluoride binder: implications on the mechanics of composite electrodes. J Power Sources 332:118–128
40. Wang H, Nadimpalli SP, Shenoy VB (2016) Inelastic shape changes of silicon particles and stress evolution at binder/particle interface in a composite electrode during lithiation/delithiation cycling. Extreme Mech Lett 9:430–438
41. Tu J, Yuan Y, Zhan P, Jiao H, Wang X, Zhu H, Jiao S (2014) Straightforward approach toward SiO2 Nanospheres and their superior lithium storage performance. J Phys Chem C 118:7357–7362
42. WN Sharpe Jr, J Pulskamp, DS Gianola, C Eberl, RG Polcawich, RJ Thompson (2006) Strain measurements of silicon dioxide microspecimens by digital imaging processing. Exp Mech. 47;(5): 649–658
43. Hutchinson JW, Suo Z (1991) Mixed mode cracking in layered materials. Adv Appl Mech 29:63–191